Mon. Not. R. Astron. Soc. 295, 156–166 (1998)

# Detection of an H92$\alpha$ recombination line in the starburst galaxy NGC 660

B. Phookun,[1]★† K. R. Anantharamaiah[2]★‡ and W. M. Goss[3]★

[1]*National Centre for Radio Astrophysics (TIFR), Pune University Campus, Ganeshkhind, Pune 411 007, India*
[2]*Raman Research Institute, Bangalore 560 080, India*
[3]*National Radio Astronomy Observatory, Socorro, NM 87801, USA*

Accepted 1997 October 16. Received 1997 August 21; in original form 1997 March 11

ABSTRACT

We have used the Very Large Array (VLA) to search for the H92$\alpha$ radio recombination line (RRL) in four starburst galaxies. In NGC 660, the line was detected over a $17 \times 8$ arcsec$^2$ region near its starburst nucleus. The line and continuum emission indicate that the RRL-emitting gas is most likely in the form of a cluster of H II regions with a small filling factor. Using a simple model we find that the total ionized mass in the nuclear region is in the range $2–8 \times 10^4$ M$_\odot$ and the rate of production of UV photons $N_{\rm Lyc} \sim 1–3 \times 10^{53}$ s$^{-1}$. The ratio of H92$\alpha$ and Br$\gamma$ line intensities in NGC 660 indicates that extinction is significant even at $\lambda = 2$ μm. The velocity field of the ionized gas is consistent with a rotating disc with an average velocity gradient of $\sim 15$ km s$^{-1}$ arcsec$^{-1}$. The dynamical mass within the central 500 pc is $\sim 4 \times 10^8$ M$_\odot$ and may be about $\sim 6 \times 10^7$ M$_\odot$ within the central 120 pc. No line was detected in the other galaxies (NGC 520, NGC 1614 and NGC 6946) to a 3$\sigma$ limit of 300 μJy. In the starburst galaxies in which RRLs have been detected, we find that there is a rough correlation between the integrated H92$\alpha$ line flux density and both the total far-infrared flux density and the radio continuum emission from the central region.

Key words: galaxies: general – galaxies: individual: NGC 660 – galaxies: starburst – radio continuum: galaxies – radio lines: galaxies.

## 1 INTRODUCTION

Until a few years ago extragalactic radio recombination lines (RRLs) had been found in only three galaxies beyond the Magellanic Clouds: M82 (Shaver, Churchwell & Rots 1977), NGC 253 (Seaquist & Bell 1977) and NGC 2146 (Puxley et al. 1991). Other searches, towards both galaxies and quasars, had yielded no significant lines (Churchwell & Shaver 1979; Bell & Seaquist 1978; Bell et al. 1984). Recently, however, the number of detections has increased to about 14 starburst galaxies (Anantharamaiah et al. 1993; Zhao et al. 1996). The reason is obvious: most of the new detections have peak strengths of about 0.5 mJy to a few mJy and widths of several hundred km s$^{-1}$, i.e. these detections are at the limits of current sensitivities. Detection of RRLs from starburst galaxies provides information about the physical conditions and kinematics of the ionized gas through an unobstructed view of the starburst activity in the nuclear regions.

In this paper, we report the results of a search for the H92$\alpha$ RRL ($\nu_{\rm rest} = 8309.3832$ MHz), made with the Very Large Array (VLA) of the National Radio Astronomy Observatory (NRAO) in Socorro, New Mexico, USA, in four starburst galaxies – NGC 660, 6946, 1614 and 520. All but NGC 660 were chosen for their intense nuclear Br$\gamma$ emission (Prestwich, Joseph & Wright 1994; Ho, Beck & Turner 1990), since the presence of the Br$\gamma$ line is an indicator of star formation, and earlier work (Anantharamaiah et al. 1993) suggested a connection between starburst activity and RRL formation. NGC 660 was chosen because it

★E-mail: bikram@ducos.ernet.in (BP);
anantha@rri.ernet.in (KRA); mgoss@aoc.nrao.edu (WMG)
†Present address: St Stephan's College, New Delhi 110 007, India.
‡Present address: NRAO, Socorro, New Mexico 87801, USA.

appears to be a merger, and is therefore the likely site of a burst of star formation. The H92α line was detected only in NGC 660.

NGC 660 is a nearly edge-on spiral galaxy at a distance of about 11 Mpc and is classified as SBa(pec) (de Vaucouleurs et al. 1991). It is a good example of the putative connection between mergers and starbursts that is apparent in computer simulations (Barnes & Hernquist 1991) and is also suggested by observations (e.g. Baum & Heckman 1989). There is direct physical evidence for a merger in NGC 660 – its nucleus has two components in the radio continuum (Condon et al. 1982) and it has a polar ring (van Driel et al. 1995; Whitmore et al. 1990), probably formed out of the gaseous debris of the merger. NGC 660 is extremely luminous in the far-infrared ($L_{\rm FIR} \sim 1.2 \times 10^{10} L_{\odot}$) (Rice et al. 1988) and in the radio (Condon 1987), both strong indicators of starburst activity.

This paper is organized as follows; the observations and results are presented in Section 2. In Section 3 the ionized gas in the nuclear region is modelled, using both the standard slab model and a collection of H II regions. In Section 4 the connection between the observed strength of RRLs and the star formation rate is examined. The paper is summarized in Section 5.

## 2 OBSERVATIONS AND RESULTS

The initial observations were made in 1995 April–May with the D configuration of the VLA of the NRAO. Follow-up observations of NGC 660 were made in 1996 March with the C array. The observing band had 16 channels covering 25 MHz with a resolution of 1.5625 MHz (56.5 km s$^{-1}$) per channel after on-line Hanning smoothing. At 8.4 GHz, the useable bandwidth (23.44 MHz) corresponds to a velocity range of $\sim$850 km s$^{-1}$. The D-array resolution with natural weighting is $\sim$10 arcsec, and the C + D-array resolution is $\sim$7 arcsec.

Four external galaxies – NGC 660, 6946, 1614 and 520 – were observed in 1995, each for about 6 h; NGC 660 was observed for an additional 2.5 h during the confirmation period in 1996. A standard VLA calibrator was observed every 20 min or so for preliminary calibration of the complex antenna gain. A strong bandpass calibrator was observed four to six times for each galaxy (except for NGC 6946, where the phase calibrator was strong enough to serve as a bandpass calibrator as well). Flux density calibration was carried out by observing 3C448 once for each galaxy. A log of the observations is given in Table 1.

The data were processed using standard procedures in the AIPS software package developed by NRAO. After correcting the complex gains of the antennas as a function of time and frequency based on observations of the calibrators, the continuum channel was self-calibrated and the solutions were applied to all the line channels. The continuum was subtracted from the line channels in the *uv* plane by fitting linear functions to the real and imaginary parts of the visibilities across channels where no line emission was expected (Cornwell et al. 1992). Since the line emission remaining after the continuum subtraction was very weak or absent, it was not necessary to deconvolve the line data cubes. In the data on NGC 660 the noise is $\sim$90 μJy beam$^{-1}$ in each channel, and in the data on NGC 520, 1614 and 6946, $\sim$100 μJy beam$^{-1}$.

Table 1. Log of VLA observations.

| Galaxy | Array | α(1950) | δ(1950) | $V_{hel}$ (km s$^{-1}$) | φ-cal | BP-cal |
|---|---|---|---|---|---|---|
| NGC 660 | D, C | 01 40 21.7 | 13 23 39.0 | 850 | 0119+041 | 0316+041 |
| NGC 1614 | D | 04 31 35.7 | –08 40 57.0 | 4778 | 0420-014 | 0316+413 |
| NGC 520 | D | 01 21 59.4 | 03 32 13.0 | 2217 | 0119+041 | 0316+413 |
| NGC 6946 | D | 20 33 49.2 | 59 58 50.0 | 50 | 2021+614 | 2021+614 |

### 2.1 H92α line emission and kinematics in NGC 660

The H92α line was detected in the nuclear region of NGC 660. The line emission extends over a region of approximately 17 × 8 arcsec$^2$ and thus the emission is resolved by the 7 arcsec beam. In Fig. 1, we show the line emission region (in grey-scale) superposed over the continuum emission (represented by contours). The line emission shows two peaks, separated by about 7.5 arcsec roughly along the major axis of the galaxy, and a slightly extended weaker line emission region underlying the two peaks. The stronger peak in the line emission is close to the continuum peak and the secondary peak is to the south-west of the continuum peak. It should be noted that the two peaks in the line emission separated by 7.5 arcsec are barely resolved by the 7 arcsec beam and therefore the apparent fine structure in the line emission seen in Fig. 1 (and also in Fig. 4, below) is due to noise in the pixels which are separated by 0.75 arcsec.

The H92α line profile integrated over the entire line emission region is shown in Fig. 2. This line profile has a peak of about 0.6 mJy at a heliocentric velocity of 850 km s$^{-1}$ and a width of about 400 km s$^{-1}$. Although it appears from Fig. 2 that there are hardly any channels at each end of the profile to determine the continuum level, the baseline in Fig. 2 has been drawn based on an examination of the line profiles at different pixels over the continuum source and also in the off-source region. Since there is a velocity structure over the continuum source, the peak of the line emission shifts within the observing band leaving discernible baselines at least at one end of the profile (e.g. Fig. 3b). In Fig. 3, we show line profiles made over 10-arcsec regions centred on the two line emission peaks and also at a position between the peaks. It is clear that the two peaks in the line emission are separated in velocity by about 200 km s$^{-1}$. The weak extended line emission underlying the two peaks is dominated by a narrow component which is unresolved with a velocity resolution of 56.5 km s$^{-1}$ (see Fig. 3c). The continuum and line parameters of NGC 660 are summarized in Table 2.

Fig. 4 shows the observed H92α velocity field (first moment) superposed on a grey-scale image of the integrated line emission (zeroth moment). The heliocentric velocity centroid of 850 km s$^{-1}$ is consistent with H I and CO velocities (van Driel et al. 1995). The centroid velocity of 850 km s$^{-1}$ corresponds to a position which is offset with respect to the continuum peak. It therefore appears that the dynamical centre of NGC 660 is offset from the continuum peak as in the case of NGC 253 (Anantharamaiah & Goss 1996). The velocity field in Fig. 4 indicates a rotating disc.

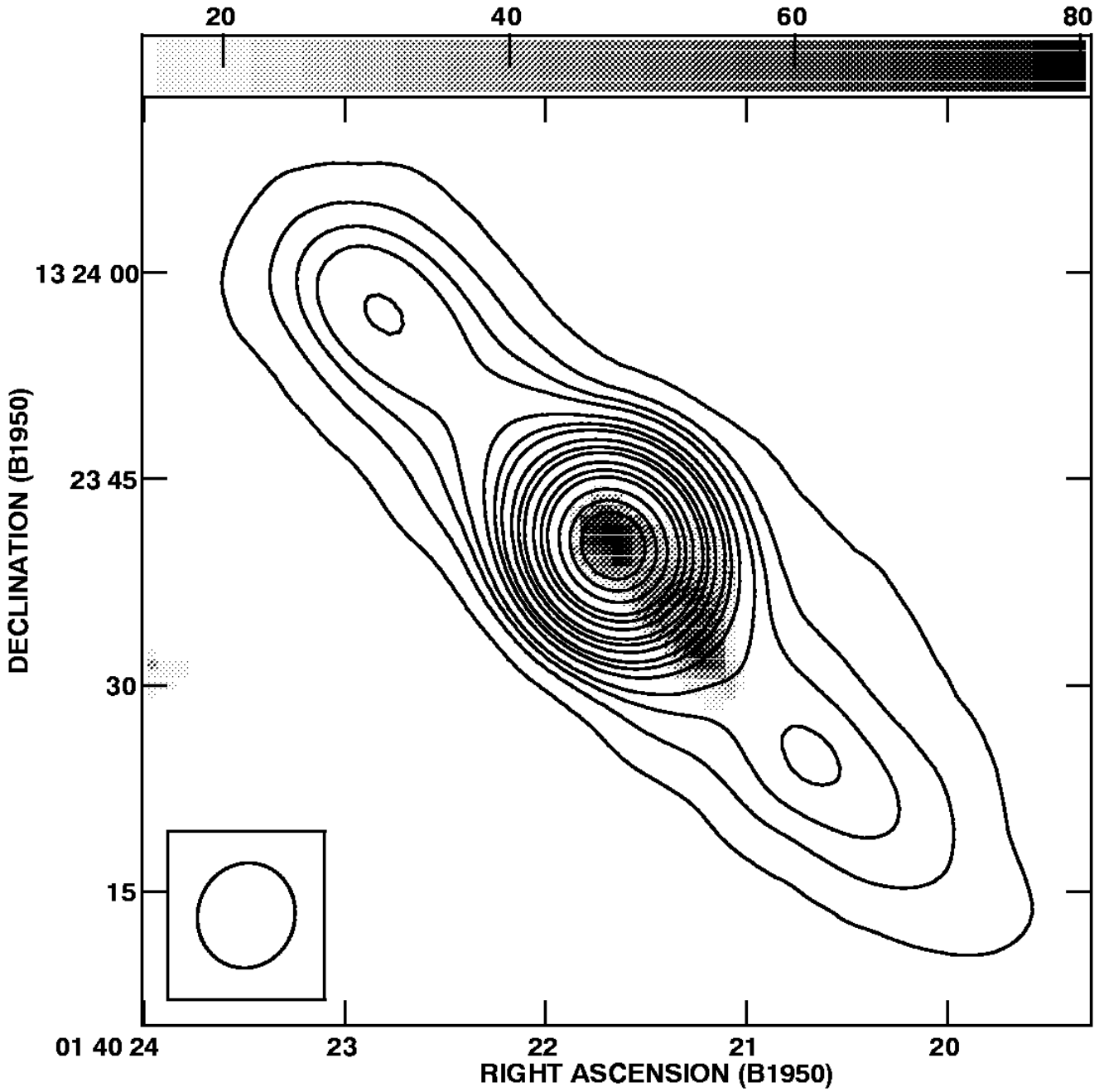


Figure 1. H92$\alpha$ line emission integrated over velocity (moment 0) from NGC 660 (grey-scale) superposed over the continuum emission at 8.3 GHz (contours). The beam shown at the bottom left corner is $7.7 \times 7.1$ arcsec$^2$ (PA $= -16°$). The grey-scale range is from 15 Jy beam$^{-1}$ ms$^{-1}$ to 80 Jy beam$^{-1}$ ms$^{-1}$. The peak continuum flux density is 58.9 mJy beam$^{-1}$. The contour levels are 0.5, 1, 1.5, 2, 3, 4, 5, 7, 9, 11, 15, 19, 23, 31, 39, 47 mJy beam$^{-1}$.

Some non-circular motions may also be present since the isovelocity contours do not run parallel to the minor axis. The average velocity gradient along the major axis is $\sim 15$ km s$^{-1}$ arcsec$^{-1}$, which is consistent with the gradient observed in H$\alpha$ by van Driel et al. (1995). The implied dynamical mass is about $4 \times 10^8$ M$_\odot$ within the central 500 pc. Although the angular resolution is only 7 arcsec, Fig. 4 indicates that within a few arcsec of the dynamical centre the velocity gradient may be steeper, approaching about 40 km s$^{-1}$ arcsec$^{-1}$. This steep gradient implies a dynamical mass of $\sim 6 \times 10^7$ M$_\odot$ within the central 120 pc.

### 2.2 Non-detections

The H92$\alpha$ line was not detected in the three other galaxies (NGC 520, 1614 and 6946) that were observed. The 3$\sigma$ upper limit to the line strengths is $\sim 150$ μJy beam$^{-1}$ for an assumed line width of 300 km s$^{-1}$. The continuum images of

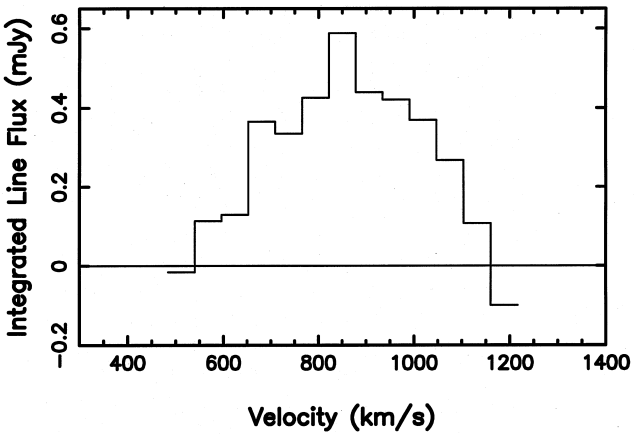


Figure 2. H92α line profile towards NGC 660 obtained by integrating a $17 \times 8$ arcsec$^2$ region corresponding to the region shown in grey-scale in Fig. 1.

these galaxies are shown in Fig. 5. These images are among the most sensitive available at 8.3 GHz, with noise levels of about 30 μJy beam$^{-1}$. The observed parameters of the three galaxies are summarized in Table 2.

## 3 MODELLING THE IONIZED GAS

In early theoretical work on extragalactic RRLs (Shaver 1978), it was predicted that externally stimulated emission – caused, for example, by the radio radiation passing through the ionized gas expected around an active nucleus – would produce detectable lines from external galaxies. The intensity of the line would be a function only of the strength of the background continuum source and would be independent of its distance, since, in stimulated emission, the line strength depends only on the path-length along the line of sight. Since a majority of the non-thermal radio sources become stronger at low frequencies, and the optical depths of the lines are very small ($10^{-3}$–$10^{-4}$), extragalactic RRL emission was expected to be preferentially observable at low frequencies. The spontaneous emission due to the ionized gas and the internally stimulated emission due to the free–free continuum generated within the ionized gas were expected to be negligible except for the nearest galaxies.

Recent observations of extragalactic RRLs show that, in a majority of the cases, the lines, contrary to expectations, are stronger at high frequencies, where the externally stimulated component is well below the limits of observation (Anantharamaiah et al. 1993; Seaquist, Kerton & Bell 1994; Zhao et al. 1996). It appears that spontaneous emission and internally stimulated emission from ionized gas are responsible for most of the observed extragalactic RRLs.

### 3.1 Uniform-slab and many-H II-region models

RRLs can be used to constrain physical conditions in the line-emitting gas. Of course, a number of assumptions must be made if only one RRL is observed, as is the case for NGC 660. In NGC 3628, NGC 1365 and IC 694, Anantharamaiah et al. (1993) found that the ionized gas, if regarded as a single slab, produced an excess of thermal continuum emisson, usually more than the total observed (thermal + non-thermal) radio emission at a given frequency. This predicted thermal emission is in conflict with the non-thermal spectral index observed over a range of frequencies. To explain the RRLs, they proposed another model for the line-emitting gas – a cluster of H II regions in the nuclear region. The two models are discussed below in more detail (see also Anantharamaiah et al. 1993 and Zhao et al. 1996). The basic equation for RRL emission is the following:

$$S_{\rm L} = \frac{2kv^2}{c^2}\,\Omega_{\rm L} T_{\rm e} \left\{ \frac{b_m \tau_{\rm L}^{*} + \tau_{\rm C}}{\tau_{\rm L} + \tau_{\rm C}} \left[1 - {\rm e}^{-(\tau_{\rm L}+\tau_{\rm C})}\right] - (1 - {\rm e}^{-\tau_{\rm C}}) \right\} + S_{\rm Cbg}\,{\rm e}^{-\tau_{\rm C}}({\rm e}^{-\tau_{\rm L}} - 1). \quad (1)$$

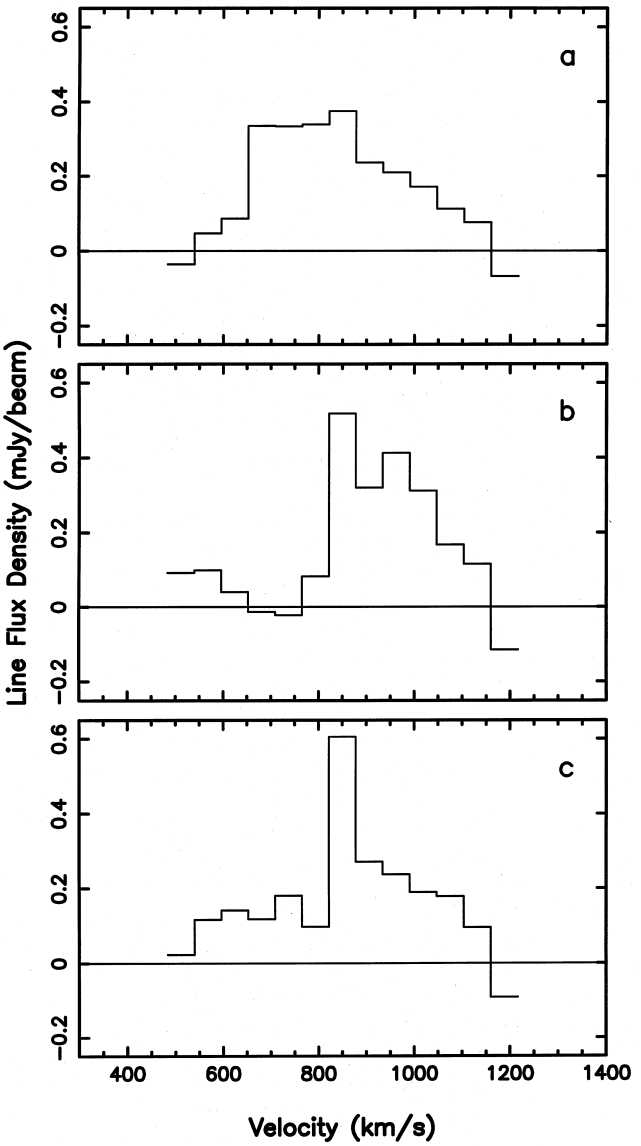


Figure 3. H92α line profiles of NGC 660 over three 10-arcsec regions centred on (a) the main peak of line emission (see Fig. 1) at an offset of $\Delta\alpha = -0.8$ arcsec and $\Delta\delta = 0.8$ arcsec from the continuum peak at $(\alpha, \delta) = 1^{\rm h}40^{\rm m}21\overset{\rm s}{.}649$, $13°23'33\overset{''}{.}8$, (b) the secondary peak in line emission at an offset of $\Delta\alpha = -5.4$ arcsec and $\Delta\delta = 4.5$ arcsec and (c) the weak extended line emission at $\Delta\alpha = -4.6$ arcsec and $\Delta\delta = 0$ arcsec.

Table 2. Observed line and continuum parameters.

| Parameter | NGC 660 | NGC 1614 | NGC 520 | NGC 6946 |
|---|---|---|---|---|
| Peak line flux density ($\mu$Jy/beam) | 500 | $< 170^1$ | $< 130^1$ | $< 120^1$ |
| Integrated line flux density ($10^{-23}$ W m$^{-2}$) | 5.6 | – | – | – |
| Continuum flux density over line region (mJy) | 71 | – | – | – |
| Peak continuum flux density (mJy/beam) | 58.9 | 37.8 | 46.0 | 26.7 |
| Total continnum flux density (mJy) | 110 | 43 | 55 | 63 |
| Centroid heliocentric velocity (km s$^{-1}$) | 850 | – | – | – |
| Beam size | 7.″7 ×7.″1 | 13.″0 × 9.″5 | 11.″0 × 9.″5 | 9.″9 × 9.″7 |
| Beam position angle | −16.°2 | −11.°8 | −8.°3 | 16.°7 |
| No. of beams covering line region | 2.8 | – | – | – |
| Line width (km s$^{-1}$) | 377 | – | – | – |
| Distance (Mpc) | 11.3 | 63.7 | 29.3 | 7.1(?) |
| Continuum flux density at 1.5 GHz (mJy) | 200[2] | 106[2] | 110[2] | 42[3] |
| Continuum flux density at 4.9 GHz (mJy) | 95[4] | 45[2] | 62[2] | 39[4] |

[1] $3\sigma$ limit (for $\Delta V = 300$ km s$^{-1}$).
[2] Hummel et al. (1987).
[3] Condon et al. (1982).
[4] Hummel, van der Hulst & Dickey (1984).

The first term represents the line emission in the ionized gas, including the stimulated emission arising from its own continuum, and the second term represents the stimulated emission due to the background continuum source. The symbols used in equation (1) are as follows: $S_L$ is the observed peak line flux, $S_{Cbg}$ the background component of the continuum flux $S_C$, $k$ the Boltzmann constant, $c$ the speed of light, $\Omega_L$ the effective solid angle of the line-emitting region, $\nu$ the frequency of observation, $T_e$ the electron temperature, $\tau_C$ the continuum optical depth, $\tau_L^*$ the peak line optical depth under LTE, and $\tau_L$ the peak line optical depth corrected for non-LTE effects ($\tau_L = b_n \beta_n \tau_L^*$, where $b_n$ is the departure coefficient and $\beta_n = 1 - (kT_e/h\nu)(\mathrm{d} \ln b_n / \mathrm{d}n)$. The peak line optical depth contains information about the width of the line ($\Delta V_{obs}$). Equation (1) is discussed in detail in several theoretical papers on RRL emission (e.g. Shaver 1975; Viner, Valee & Hughes 1979; Roelfsema & Goss 1992). The departure coefficients used in our models are from Salem & Brocklehurst (1979). In addition to the line emission, there is radio continuum emission over a range of frequencies associated with the line-emitting region. This continuum emission is usually primarily non-thermal as evidenced by the spectral index, but the continuum must have a thermal component because of the hot gas that is responsible for the line. This thermal emission is given by

$$S_{th} = \frac{2k\nu^2}{c^2} \Omega_L T_e (1 - e^{-\tau_C}). \quad (2)$$

The observed parameters are $S_L$, $\Delta V_{obs}$ and $S_C$. The model parameters which are to be determined are the electron temperature and density, $T_e$ and $n_e$, and the distribution of the gas, subject to reasonable physical constraints. A single ($T_e$, $n_e$) pair characterizes a particular realization of each model; this is rather simplistic, but justified, since we have only one RRL detection to model. A more elaborate, multi-component model may be necessary when several RRL detections are made in a galaxy. In the slab model we begin with a slab that has the same lateral size as the line-emitting region, and with three parameters, the electron temperature and density $T_e$ and $n_e$, and the path-length ($l$) through the slab along the line of sight. Of the three unknown parameters, we choose $T_e$ and $n_e$ in pairs and determine $l$. The background continuum source is assumed to create the entire continuum flux when calculating the stimulated emission, i.e. $S_{Cbg}$ is set equal to $S_C$ in the last term of equation (1). This assumption is justified at high frequencies and high densities, where the contribution of the term involving $S_{Cbg}$ is negligible, but it has to be modified at low frequencies ($< 12.4$ GHz) or low densities, at which the contribution of stimulated emission arising from the background source can become important. The parameters of the ionized gas ($T_e$,

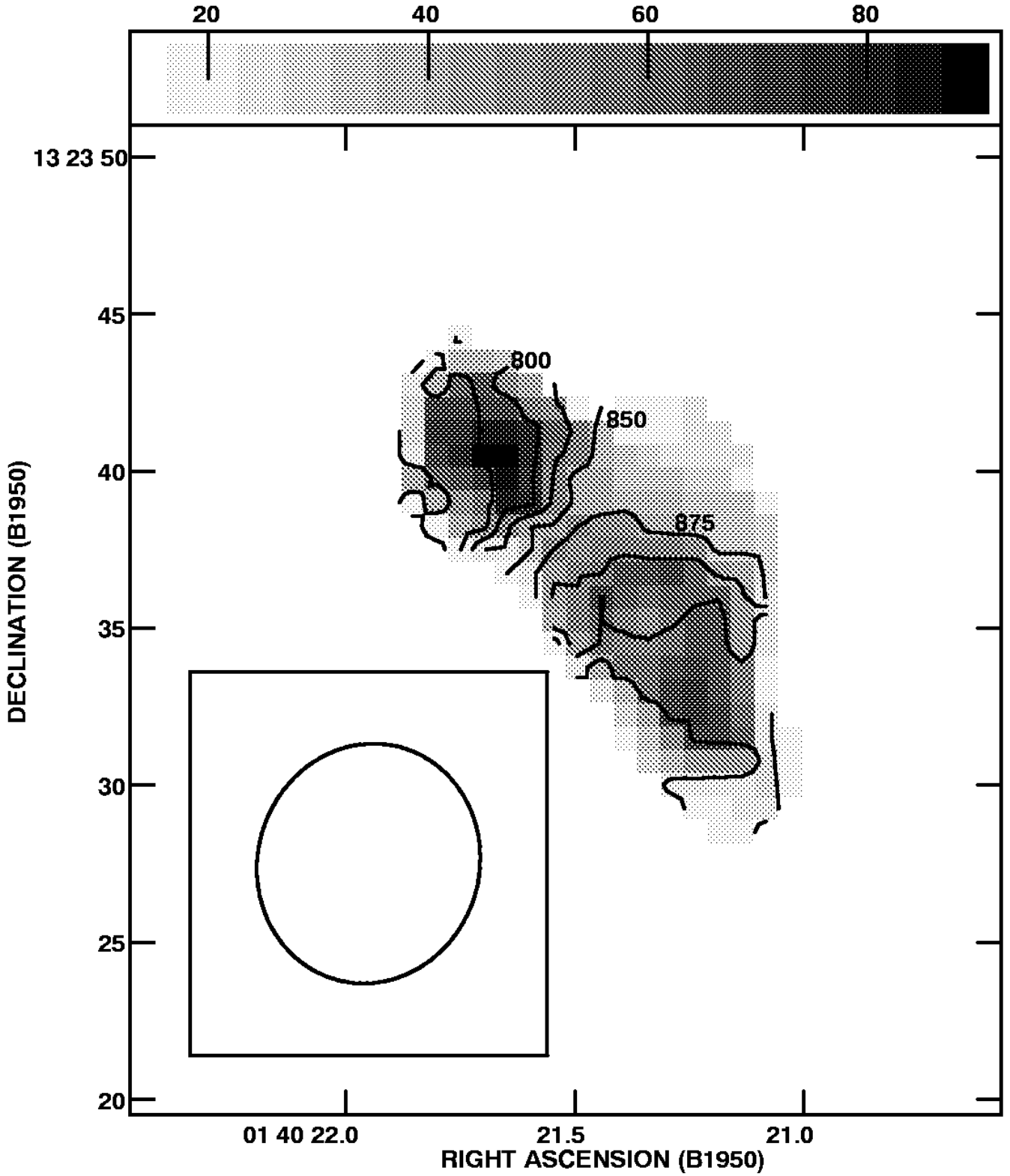


Figure 4. The heliocentric velocity field (contours) in the central region of NGC 660 observed in the H92α line superposed on the integrated line emission (moment 0) in grey-scale. Contour levels are labelled in units of km $s^{-1}$. Contour intervals are 25 km $s^{-1}$.

$n_e$, $l$) are then used to calculate the total thermal continuum emission arising from the slab using equation (2). In the model containing many H II regions, we have of course the same observed parameters. Here the peak line emission for each H II region ($S_L^{H\,II}$) is calculated separately: $\Omega_L$ is replaced by $\Omega_{H\,II}$, the angular extent of each H II region, in the first term of equation (1), and the second term is multiplied by $(1/2)(\Omega_{H\,II}/\Omega_L)$, to scale down the background con-

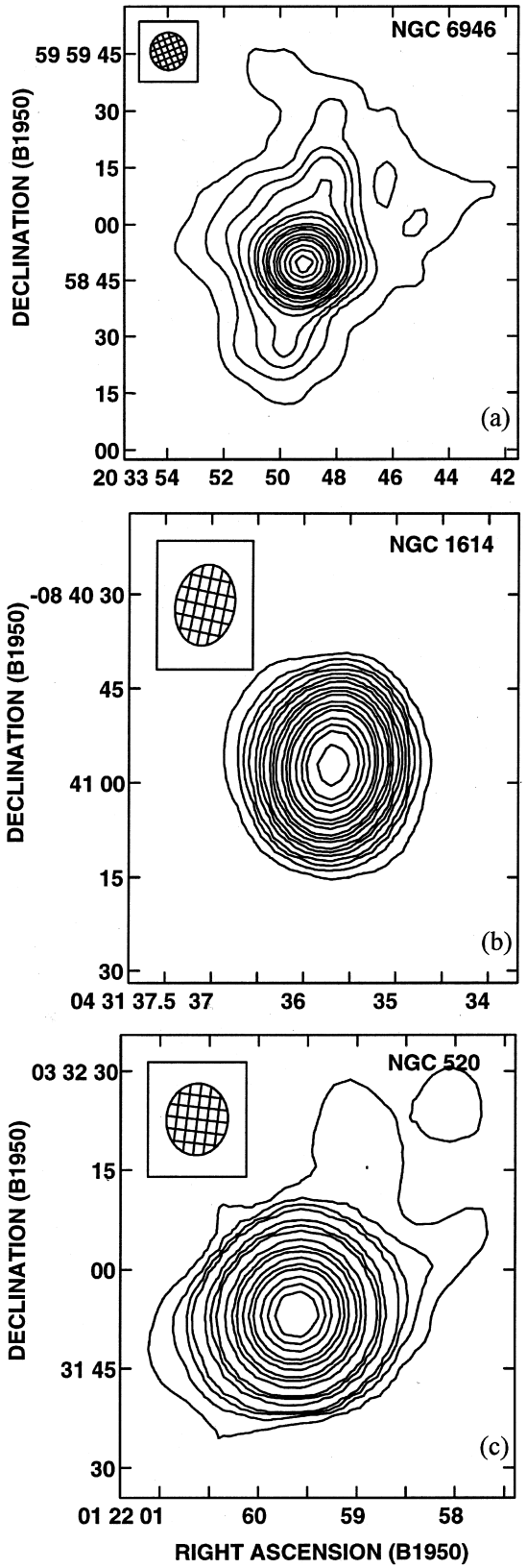


tinuum flux $S_{\rm Cbg}$ shining upon a single H II region, on the assumption that, on average, half the radiation observed along a line of sight arises behind the H II region. The H II regions are assumed to be identical in size, electron temperature and electron density, all three of which are free parameters of this model. The total number ($N$) of H II regions is obtained by dividing the observed integrated line flux density by the integrated line flux density of each H II region in the model (the peak flux of which is constrained to be less than the peak flux of the observed line). The size and number of H II regions also yields a filling factor for the H II regions, since the maximum volume that can be occupied by these regions is the volume of the line-emitting region ($\sim L^3$). The filling factor is constrained to be $<1$, thus setting an upper limit on $N$; a lower limit is set by the requirement that a minimum number of H II regions must exist within each beam area for the observed average velocity width of the line to be filled by the line profiles of the individual H II regions. In this model the line emission is taken to be the sum of the contributions of the individual H II regions, which is not quite correct if the H II regions shadow one another. If, however, the filling factor is small, as it is in most of the realistic models (see Anantharamaiah et al. 1993 and Zhao et al. 1996), then there is very little actual shadowing – i.e. every H II region is visible along some line of sight – and it is not necessary to correct for shadowing. Similarly, in calculating the total thermal continuum emission from the H II regions, the correct procedure is to calculate the flux density for each H II region (using equation 2, with $\Omega_{\rm H\,II}$ substituted for $\Omega_{\rm L}$) and to use the effective optical depth along each line of sight to determine how many H II regions are visible. In the model used, the effective optical depth is calculated by assuming that the H II regions are randomly distributed in the line-emitting region (see Anantharamaiah et al. 1993). We find that in most of the models that satisfy the constraints, the filling factors are very small and essentially all the H II regions are visible. The total thermal emission should of course be less than the total continuum emission; if an estimate of the thermal emission is available, e.g. from Br$\gamma$ observations (Ho et al. 1990; Prestwich et al. 1994), then this estimate is used as a constraint. In addition, the total continuum emission measured at other frequencies is used to constrain the models in the following way. At every frequency, including the frequency of the observed RRL, the total observed continuum flux density is the sum of thermal and non-thermal components, i.e. $S_{\rm obs}=S_{\rm nth}+S_{\rm th}$. Since the model provides an $S_{\rm th}$ at every frequency, it is possible to use every $S_{\rm obs}$ to get the corresponding $S_{\rm nth}$. Two of these non-thermal fluxes are used to derive a non-thermal spectral index $\alpha$. We thus get a model-based expected variation of the total continuum flux density with frequency which is compared with the measured values to obtain further constraints on the model.

The major difference between the slab model and the many-H II-region model lies in the distribution of the ion-

Figure 5. Continuum images of three galaxies from which the H92$\alpha$ line was not detected. The images were made using natural weighting. (a) NGC 6946, with a peak flux density of 26.7 mJy beam$^{-1}$. The beam size is $9.9 \times 9.7$ arcsec$^2$. The first contour and the contour intervals are 0.25 mJy beam$^{-1}$. Contour intervals double at 4th, 7th, 10th, 13th and 17th contours. (b) NGC 1614, with a peak flux density of 37.8 mJy beam$^{-1}$. The beam size is $13.0 \times 9.5$ arcsec$^2$ with position angle $-12°$. Contour levels are the same as (a). (c) NGC 520, with a peak flux density of 46 mJy beam$^{-1}$. The beam size is $10.9 \times 9.4$ arcsec$^2$ with position angle $-7°$. Contour levels are 0.1, 0.2, 0.3, 0.4, 0.8, 1.2, 1.6, 3.2, 4.8, 6.4, 9.6, 12.8, 16, 22.4, 28.4 and 34.8 mJy beam$^{-1}$.

ized gas. The slab model uses a uniform distribution of the line-emitting region and only adjusts the depth along the line of sight. On the other hand the many-H II-region model allows the gas to be distributed in a number of clumps (with only an average uniformity) over the central region. If the gas is optically thin, the difference between the models for the line and thermal continuum emission is negligible; however, if the individual H II regions become optically thick, the second model produces more line emission for a given amount of thermal continuum emission.

### 3.2 Results of model calculations

In applying the above two types of models, we considered electron temperatures ($T_e$) in the range 1000 to 12 500 K, electron densities ($n_e$) in the range 10 to $10^6$ cm$^{-3}$, and H II region diameters ($l$) ranging from 0.01 to 10 pc. Since the models are being fitted to a single weak line, it is possible to obtain acceptable solutions for a range of parameters. We first discuss the general nature of the solutions and then propose plausible values of the H II region parameters.

We find that the slab model is not satisfied for any $T_e > 2500$ K. For $T_e \geq 5000$ K, the model produces too much thermal continuum emission, amounting to essentially all the continuum emission, especially when $T_e \sim 10\,000$ K.

In the many-H II-region model, we find that the low-temperature ($T_e = 1000$, 2500 K) models can be satisfied for a wide range of densities and sizes. These models, however, have the fundamental problem that a temperature below 3000 K is not likely unless the abundance of heavy elements is uncommonly high and cooling mechanisms extraordinarily efficient (Churchwell et al. 1978; Shaver et al. 1983). Furthermore, if the H II regions are associated with a starburst, then their temperatures are unlikely to be lower than $\sim$5000 K; H II regions in our galaxy have temperatures between 4000 and 9000 K (Afflerbach et al. 1996). Among models with $T_e \geq 5000$ K, the high-density cases have turnover frequencies close to or higher than the highest frequency at which continuum measurements are available; for example, a 1-pc H II region with $T_e = 10\,000$ K and $n_e = 10^4$ cm$^{-3}$ has a turnover frequency of $\sim$5.3 GHz. As a result the very high density models suggest relatively high thermal continuum flux densities at higher frequencies. In most galaxies, however, we expect the total continuum emission to have a non-thermal-type spectrum all the way to $\sim$50 GHz (see Condon 1992).

There is a small range in temperatures, densities, and sizes in which the continuum spectrum remains non-thermal-like all the way to 50 GHz, and in which the temperatures are $\geq$5000 K; the densities corresponding to these models are $\sim$10 000 cm$^{-3}$, and the sizes of the individual H II regions are about 1 pc. The ionized gas may be described as consisting of small, optically thick H II regions that sparsely fill the region from which the line is observed. As a result of the high opacity of the individual H II regions, the line is essentially formed only in the surface layer of each H II region; the line strength is thus proportional to the surface area of the ionized gas (rather than to the volume, as it would be in the case of optically thin gas). The low filling factor ensures that virtually all the radiation – line and continuum – produced by the individual H II regions escapes without being absorbed. The contribution of external stimulation emission is found in all cases, optically thin or thick, to be negligible. The major contribution to the line flux density comes from internal stimulated emission in the H II regions: in the optically-thick models that are supported by the data, the continuum emission generated in the interior of an H II region acts as the input to the maser in the outer layers.

The expected variation of line and continuum strengths as a function of frequency are shown for two such models in Fig. 6. It is evident from Fig. 6 that a second RRL measurement at a lower frequency would be valuable in constraining the models. The parameters of the two models, A and B, shown in Fig. 6 are summarized in Table 3. For temperatures higher than or equal to 5000 K, the range of parameters allowed by the constraints are rather small. Over the grid of values of $T_e$ and $n_e$ that were explored, acceptable models were found only for $T_e = 5000$ and 7500 K, and at each of these temperatures the allowed values of the electron density are $n_e = 5000$ and $10^4$ cm$^{-3}$. Models with higher densities predicted optically-thick thermal spectra for the continuum emission at frequencies higher than 10 GHz. Lower density models were ruled out since they produced too much thermal emission at centimetre wavelengths which is inconsistent with the observed non-thermal spectrum. Within the acceptable models, the ranges of the derived parameters are: $M_{\rm H\,II} \sim 2$–$8 \times 10^4\,{\rm M}_\odot$, $N_{\rm Lyc} \sim 1$–$3 \times 10^{53}$ s$^{-1}$ and the expected Br$\gamma$ line flux $\sim 1$–$2 \times 10^{-13}$ erg s$^{-1}$ cm$^{-2}$.

In both the slab model and the many-H II-region model, we have considered only a single component of ionized gas with a given combination of $T_e$ and $n_e$. A more realistic model would incorporate more than one component to the ionized gas. The single frequency data that we have here do not, of course, justify a complex model. The kind of model that we believe our RRL data support – a cluster of H II regions – can be considered an approximate representation of a star-forming region. The process of star formation has been studied extensively in a large number of galaxies. In Section 4 we attempt to trace the link between RRLs and star formation.

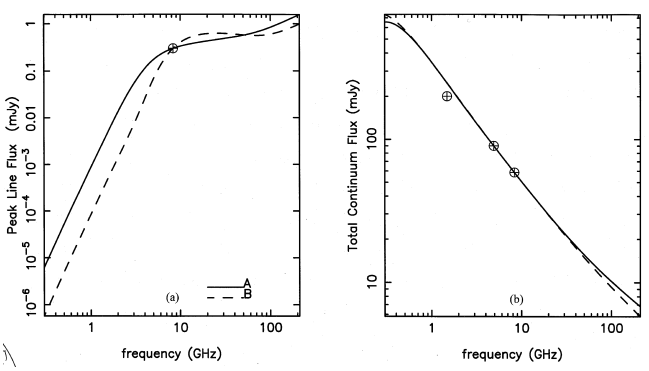


Figure 6. Predicted variation as a function of frequency of (a) peak recombination line flux density assuming a fixed line width of 375 km s$^{-1}$ and (b) sum of thermal and non-thermal continuum flux density from the line-emitting region based on two typical models with a collection of H II regions in the nuclear region of NGC 660. The parameters of the models are given in Table 2. The solid line represents model A and the dashed line represents model B.

Table 3. Model parameters for NGC 660.

| Parameter | Model A | Model B |
|---|---|---|
| Electron temperature (K) | 5000 | 5000 |
| Electron density ($cm^{-3}$) | 5000 | 10000 |
| Size of an HII region (pc) | 1.0 | 1.0 |
| Number of HII regions | 1044 | 158 |
| Filling factor | $4 \times 10^{-6}$ | $6 \times 10^{-7}$ |
| $\tau_C^{HII}$ (5 GHz) | 0.70 | 2.8 |
| $\tau_C^{HII}$ (8.3 GHz) | 0.24 | 0.95 |
| $\tau_L^{HII}$ (8.3 GHz) | −0.65 | −1.5 |
| Stimulated emission % | 0.7 | 0.2 |
| $S_{th}^{5GHz}$ (mJy) | 12.3 | 3.5 |
| $S_{nth}^{5GHz}$ (mJy) | 81.6 | 90.4 |
| Spectral Index ($\alpha_{nth}$) | −0.73 | −0.67 |
| Total mass of ionized gas ($10^4\ M_\odot$) | 6.7 | 2.0 |
| $N_{Lyc}$ ($10^{53}$ $s^{-1}$) | 1.8 | 1.1 |
| Number of O5 stars | 3890 | 2360 |
| Br$\alpha$ flux ($10^{-13}$ ergs $s^{-1}$ cm−2) | 5.8 | 3.5 |
| Br$\gamma$ flux ($10^{-13}$ ergs $s^{-1}$ cm−2) | 1.9 | 1.1 |

### 3.3 Constraints from non-detections

It is also possible to use the upper limits on the RRL emission from NGC 520, 1614 and 6946, in conjunction with continuum and other line observations, to place some constraints on the conditions in these galaxies. We can model the gas as in NGC 660, using the $3\sigma$ limits as the peak line strengths and assuming line widths of 300 km $s^{-1}$. (Armus, Heckman & Miley 1990 find that the [O III] line widths of the nuclear regions of active and starburst galaxies have a median value of 300 km $s^{-1}$.) In these models, we assume the line-emitting region to be about one resolution element (i.e. a few hundred pc to a few kpc, depending on the distance), which is the typical size of a nuclear starburst. The parameters of typical models are summarized in Table 4. We have shown those models that predict an upper limit to the Br$\gamma$ flux which is in agreement with the observed values (Ho et al. 1990; Prestwich et al. 1994). Considering the many uncertainties in modelling with non-detections, these calculations should be taken primarily as a check for consistency of the non-detections with the known properties of the galaxies.

Table 4. Model parameters for non-detections.

| Parameter | NGC 520 | NGC 1614 | NGC 6946 |
|---|---|---|---|
| Electron temperature (K) | 7500 | 7500 | 7500 |
| Electron density ($cm^{-3}$) | 1000 | 1000 | 1000 |
| Size of an HII region (pc) | 1.00 | 2.5 | 1.0 |
| Assumed size of line region (kpc) | 1.4 | 3.4 | 0.3 |
| Number of HII regions | $< 1.7 \times 10^5$ | $< 5.7 \times 10^4$ | $< 9.3 \times 10^3$ |
| Total mass of ionized gas ($10^6\ M_\odot$) | < 2.2 | < 11.5 | < 0.12 |
| $N_{Lyc}$ ($10^{53}$ $s^{-1}$) | < 8.6 | < 45 | < 0.5 |
| Br$\alpha$ flux ($10^{-13}$ ergs $s^{-1}$ $cm^{-2}$) | < 4.2 | < 4.6 | < 3.9 |
| Br$\gamma$ flux ($10^{-13}$ ergs $s^{-1}$ $cm^{-2}$) | < 1.3 | < 1.5 | < 1.2 |

## 4 RADIO RECOMBINATION LINES AND STAR FORMATION

In selecting the galaxies observed in this paper, we used the starburst phenomenon as a way of pointing to the existence of radio recombination lines, i.e. we expected the star formation rate (SFR) to be correlated with the RRL strength. To check the extent to which this is true, it is useful to plot the observed RRL strength against one of the two most dependable indicators of star formation rate, the radio continuum emission and the far-infrared (FIR) emission. (Condon 1992 has presented an excellent discussion of the various indicators of star formation.)

In Figs 7(a) and (b), we plot the integrated H92$\alpha$ flux density (11 detections and five upper limits) against the flux and the radio continuum flux density at 8.4 GHz from the central regions of starburst galaxies. The H92$\alpha$ line data and the radio continuum data are taken from Anantharamaiah et al. (1993), Zhao et al. (1996) and from some further unpublished work by the same authors. The FIR fluxes in Fig. 7(a) were taken from the reference catalogue of de

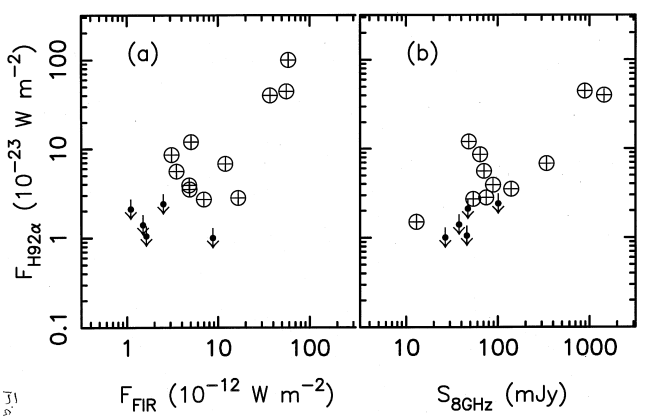


Figure 7. Integrated flux density of H92$\alpha$ recombination line plotted against (a) total FIR flux density given in de Vaucouleurs et al. (1991) and (b) radio continuum flux density at 8 GHz from the nuclear region of starburst galaxies. The recombination line and radio continuum data are taken from Anantharamaiah et al. (1993), Seaquist et al. (1994) and Zhao et al. (1996).

Vaucouleurs et al. (1991). The FIR fluxes are the average of the flux densities in the 60- and 100-μm bands observed by *IRAS*. It is obvious that there is a rough correlation between the RRL flux density and the other indicators of SFR. However, there is considerable scatter in the correlation. There are three reasons why, even if the presence of an RRL is related to the star-formation process, the correlation between the observed RRL flux density and the FIR or radio continuum flux density is expected to be only approximate.

(1) RRL formation is not a local thermodynamic equilibrium (LTE) process. The line emission is strongly dependent on the coefficient $\beta_n$, which varies with temperature and density (Salem & Brocklehurst 1979) and which gives rise to stimulated emission. RRLs are unlike optical and infrared recombination lines, in which, because stimulated emission is negligible, only the departure coefficient, $b_n$, is important in non-LTE situations; since $b_n$ is always close to unity, the strengths of optical and infrared recombination lines are much less sensitive to departure from LTE.

(2) We find in our models that the thermal radio continuum emission comes from optically thick H II regions. Therefore, the observed thermal component of the radio emission is not a true indicator of the SFR. The non-thermal component is, however, not affected significantly by the presence of compact H II regions since the latter have a very low filling factor in the nuclear regions.

(3) In some of the galaxies which may be harbouring a central black hole, the total non-thermal emission may have some contribution from sources unrelated to star formation. Thus, the expected correlation between the total radio emission and other indicators of star formation is weakened (Condon et al. 1982).

Optical and IR recombination lines are good indicators of the SFR if the correction arising from extinction is applied properly. The extinction correction is especially difficult for optical lines such as Hα. For example, Armus et al. (1990) have shown that in a sample of merger starbursts, the star formation rate determined from the FIR emission is an order of magnitude higher than that determined from Hα, even after aplication of the reddening correction derived from the Hα/Hβ ratio. Our models indicate (see Table 3) that IR lines also may suffer from extinction. For example, in NGC 660 our models predict a Brγ flux density which is about three times the extinction-corrected flux density given by Ho et al.

## 5 SUMMARY

As part of a programme to search for radio recombination lines in active galaxies, we used the D array of the VLA to observe the H92α line in NGC 660, 6946, 1615 and 520. The H92α line was detected only in NGC 660. The line emission is resolved with a beam of ∼7 arcsec and the velocity field of the ionized gas indicates a rotating disc. We have modelled the line-emitting region as a slab of ionized gas that is optically thin to the line and continuum emission, and as a cluster of compact H II regions that is optically thick to the continuum emission, using not only the line and continuum emission detected here but also the continuum emission observed at other frequencies. We find that the latter model provides a more satisfactory explanation of the ionized gas. One of the models that fit the observations indicates that there may be a cluster of over a thousand high-density H II regions ($n_e = 5000\ \mathrm{cm}^{-3}$), each of size 1 pc. A cluster of H II regions would be expected in a starburst scenario, and therefore we examine the RRL detections in NGC 660 and other galaxies in the context of star formation. We find that there is a rough correlation between the integrated line flux densities and both the far infrared flux densities and the radio continuum emission from the nuclear region. We argue that this is what would be expected from our present understanding of recombination lines and the process of star formation in central regions of galaxies.

## ACKNOWLEDGMENTS

We thank D. J. Saikia for useful discussions and A. L. Roy for a critical reading of the manuscript. BP thanks the Raman Research Institute for hospitality. The National Radio Astronomy Observatory is a facility of the National Science Foundation operated under cooparative agreement by Associated Universities Inc.

## REFERENCES

Afflerbach A., Churchwell E., Accord J. M., Hofner P., Hurtz S., Depree C. G., 1996, ApJS, 106, 323
Anantharamaiah K. R., Goss W. M., 1990, in Gordon M. A., Sorochenko R. L., eds, Proc. IAU Colloq. 125, Radio Recombination Lines: 25 Years of Investigation. Kluwer, Dordrecht, p. 267
Anantharamaiah K. R., Zhao J.-H., Goss W. M., Viallefond F., 1993, ApJ, 419, 585
Armus L., Heckman T. M., Miley G. K., 1990, ApJ, 364, 471
Barnes J. E., Hernquist L. E., 1991, ApJ, 336, L65
Baum S. A., Heckman T. M., 1989, ApJ, 336, 681
Bell M. B., Seaquist E. R., 1978, ApJ, 223, 378
Bell M. B., Seaquist E. R., Mebold U., Reif K., Shaver P. A., 1984, A&A, 130, 1
Churchwell E., Shaver P. A., 1979, A&A, 77, 316
Churchwell E., Smith L. F., Mathis J., Mezger P. G., Huchtmeier W., 1978, A&A, 70, 719
Condon J. J., 1987, ApJS, 65, 485
Condon J. J., 1992, ARA&A, 30, 575
Condon J. J., Condon M. A., Gisler J., Puschell J. J., 1982, ApJ, 252, 102
Cornwell T. J., Uson J. M., Haddad N., 1992, A&A, 258, 583
de Vaucouleurs G., de Vaucouleurs A., Corwin H. G., Buta R. J., Paturel G., Fouqué P., 1991, Third Reference Catalog of Bright Galaxies. Springer-Verlag, New York
Ho P. T. P., Beck S. C., Turner J. L., 1990, ApJ, 349, 57
Hummel E., van der Hulst J. M., Dickey J. M., 1984, A&A, 134, 207
Hummel E., van der Hulst J. M., Keel W. C., Kennicutt R. C., Jr, 1987, A&AS, 70, 517
Prestwich A. H., Joseph R. D., Wright G. S., 1994, ApJ, 422, 73
Puxley P. J., Brand P. W. J. L., Moore T. J. T., Mountain C. M., Nakai N., 1991, MNRAS, 248, 585
Rice W., Lonsdale C. J., Soifer B. T., Neugebauer G., Kopan E. L., Lloyd L. A., de Jong T., Habing H. J., 1988, ApJS, 68, 91
Roelfsema P. R., Goss W. M., 1992, A&AR, 4, 161
Salem M., Brocklehurst M., 1979, ApJS, 39, 633
Seaquist E. R., Bell M. B., 1977, A&A, 60, 1

Seaquist E. R., Kerton C. R., Bell M. B., 1994, ApJ, 492, 612
Shaver P. A., 1975, Pramana, 5, 1
Shaver P. A., 1978, A&A, 68, 97
Shaver P. A., Churchwell E., Rots A. H., 1977, A&A, 55, 435
Shaver P. A., McGee R. X., Newton L. M., Danks A. C., Pottasch S. R., 1983, MNRAS, 204, 53
van Driel W. et al., 1995, AJ, 109, 942
Viner M. R., Vallee J. P., Hughes C. A., 1979, AJ, 84, 1335
Whitmore B. C., Lucas R. A., McElroy D. B., Steinman-Cameron T. Y., Sackett P. D., Olling R. P., 1990, AJ, 100, 1489
Zhao J. H., Anantharamaiah K. R., Goss W. M., Viallefond F., 1996, ApJ, 472, 54